

Designing of interference pattern in ultra-short pulse laser processing

Yoshiki Nakata · Keiichi Murakawa · Kenji Sonoda ·
Kazuma Momoo · Noriaki Miyanaga ·
Takuya Hiromoto

Received: 15 December 2011 / Accepted: 3 August 2012 / Published online: 15 September 2012
© Springer-Verlag 2012

Abstract We have studied material processing by using an interfering ultra-short pulse laser. In this process, an interference pattern is transferred to material surface, and a periodic structure can be generated in a single shot of laser irradiation. Here, it is well known that the period of the interference pattern can be controlled by correlation angle and wavelength. In addition, a composite, doubled in density or designed interference pattern can be formed by controlling the phase shift and variation of amplitude between the interfering laser beams. In this paper, basic patterns of interference are summarized in the case of four-beam correlation.

1 Introduction

Nanotechnology has been a topic for over two decades. We have been working on metallic thin film processing by interfering laser to fabricate nanostructures in lattice [1–9]. Such structures are called “metamaterial”, in which a distinctive nature can be induced or enhanced. An example unit structure is nanomesh [2, 3], where nano-sized holes are ablated, which is known as MHA (metal hole array), showing the extraordinary transmission phenomenon. On the other hand, liquid motion of metal can be induced by periodic induction of energy by interference, and 3-dimensional struc-

tures such as nanobump [3], nanowaterdrop [3, 7], nanoneedle and nanowhisker [5, 8] were fabricated successfully. In short, a concave structure is fabricated according to the distribution of low fluence region, and 3-dimensional structure is fabricated according to that of high fluence region.

The unit structures, convex or concave, and the matrix decide the basic characters of the metamaterials. To control them, an interference pattern has to be designed. In the past experiments and simulations, the number of beams, amplitude difference and phase shift between the beams were useful to control the interference pattern, and some designed structures could be obtained, such as duplicated, doubled and designed structures [7, 13]. In this paper, we survey the interference pattern of four countering beams by simulation. We show 21 pictures categorized into six figures. The design of higher fluence and lower fluence is investigated in detail.

2 Calculation

Interference of laser has been applied to create periodic structures such as fiber grating, distributed-feedback laser. In case of material processing, an interference pattern of two beams was applied to direct photo-dissociation of a polymer [10]. In this simulation, we use four countering femtosecond laser beams forming a quadrangular pyramid according to our past experiments, as shown in Fig. 1 (in the case of six beams, please check the other paper [13]). They interfere through a demagnification system [2], and this configuration was firstly examined by Maznev et al. in the case of two beams [11], was applied to four beams by Kondo et al. [12], and the interference pattern in the case of six beams has been investigated by our group [13]. The femtosecond laser can achieve a resolution better than a wavelength in

Y. Nakata (✉) · K. Murakawa · K. Sonoda · K. Momoo ·
N. Miyanaga
Institute of Laser Engineering, Osaka University, 2-6 Yamadaoka,
Suita 565-0871, Japan
e-mail: nakata-y@ile.osaka-u.ac.jp
Fax: +81-6-68798729

T. Hiromoto
Furukawa Electric Col, Ltd., 6 Yawata-Kaigandori, Ichihara,
Chiba 290-8555, Japan

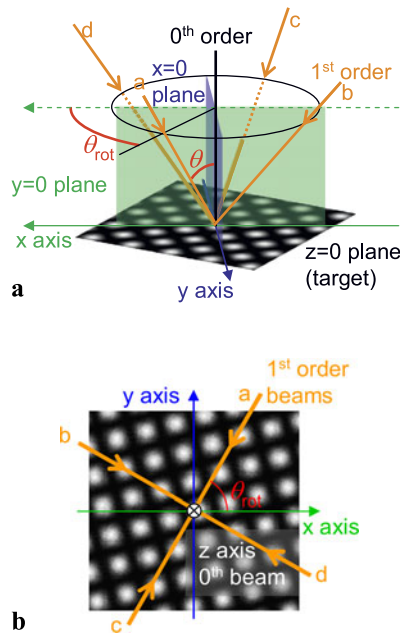


Fig. 1 Explanation of interfering four beams

material processing, so it is suitable for interfering laser processing in which the period can be shortened to wavelength.

In any case, the interference pattern of multi beams can be calculated in the following equation;

$$I = \left\langle \left| \sum_i E_i \right|^2 \right\rangle \tag{1}$$

here $\langle A(t) \rangle$ explains time average of $A(t)$. E_i explains each of the electrical fields of the beams a, b, c and d , which are illustrated in Fig. 1. We assume that four beams interfere evenly at an interference angle θ to substrate normal, where an interference pattern is projected. The rotation angle θ_{rot} is set to 0, 90, 180, 270, respectively. In this simulation, we assume a continuous wave for simplicity as follows;

$$E_i (i = a, c) = E_{i_0} \cos(k \cos \theta * z \mp k \sin \theta * x - \omega t + \phi_i) \tag{2}$$

$$E_i (i = b, d) = E_{i_0} \cos(k \cos \theta * z \mp k \sin \theta * y - \omega t + \phi_i) \tag{3}$$

Table 1 Shapes of higher- and lower-fluence regions

Figure	Higher fluence	Lower fluence	E_a	E_b	E_c	E_d	ϕ_a/π	ϕ_b/π	ϕ_c/π	ϕ_d/π
2(a)	Circle/round box	Mesh	1	1	1	1	0	0	0	0
2(b)	Circle/round box	Mesh	1	1	1	1	0	0.25	0.25	0.25
2(c)	Circle/mesh	Four countering ellipses	1	1	1	1	0	0.5	0.5	0.5
2(d)	Circle/mesh	Four countering ellipses/boxes	1	1	1	1	0	0.75	0.75	0.75
2(e)	Double/check	Double/check	1	1	1	1	0	1	1	1
3(a)	Ellipse	Ellipsoidal mesh	1	1	1	1	0	0.5	0.5	0
3(b)	Ellipse	Triangle mesh in hexagon	1	1	1	0	0	0.5	0.5	0
3(c)	Ellipse	Wave/ellipsoidal mesh	1	1	0.5	0.5	0	0.5	0	0.5
3(d)	Ellipse/linear beads	Wave/ellipsoidal mesh	1	1	0.5	0.5	0	0.5	0	1
3(e)	Ellipse/cat's eye/pea	Ellipse/cat's eye/pea	1	1	0.5	0.5	0	0.5	0.5	1
4(a)	Circle/droplet	Triangle mesh/mesh	1	1	1	0.5	0	1	0.5	1
4(b)	Circle/droplet	Triangle mesh/mesh	1	1	1	0.5	0	1	0.5	0
4(c)	Circle/droplet	Triangle mesh/mesh	1	0.5	1	1	0	1	0.5	0
4(d)	Circle/droplet	Triangle mesh/mesh	1	0.5	1	1	0	1	0.5	1
4(e)	Pea/ellipse	Star cross/ellipse	1	0.5	1	0.5	0	0.5	0.5	0
5(a)	Peanuts	Round triangle mesh on hexagon/peanuts mesh	1	1	0.5	1	0	0.5	0.5	1
5(b)	Peanuts	Round triangle mesh on hexagon/peanuts mesh	1	0.5	1	1	0	0.5	0.5	1
5(c)	Round triangle mesh on hexagon/peanuts mesh	Peanuts	1	0.5	0.5	0.5	0	1	1	1
6	Round half-moon, wave, step	Round half-moon, wave, step	1	0.5	1	0.5	0	0	0.5	0.5
7(a)	Round triangle	Mesh, boomerang	1	0.5	0.5	0.5	0	0.5	0.5	0.5
7(b)	Round trapezoid	Mesh, gull	1	0.5	1	0.5	0	0	0.5	1

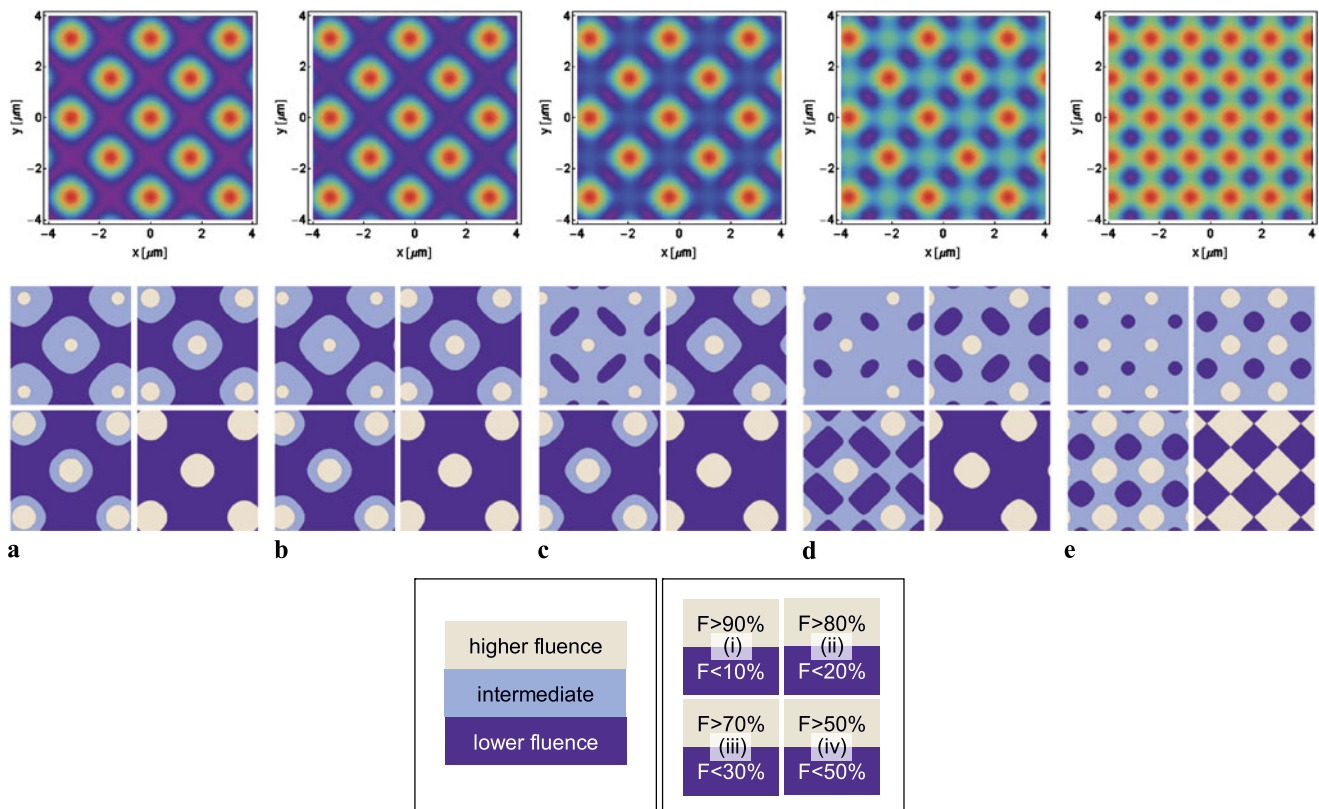


Fig. 2 Interference patterns as a function of phase shift. (a) $\Delta\phi_a = 0$, (b) $\Delta\phi_a = \frac{1}{4}\pi$, (c) $\Delta\phi_a = \frac{2}{4}\pi$, (d) $\Delta\phi_a = \frac{3}{4}\pi$, and (e) $\Delta\phi_a = \pi$. Top pictures are simulated interference pattern. Sets of four pictures in the middle are corresponding contour plots at different thresholds. Bottom

inserts explain the thresholds of the contour plots: (i) (90 %, 10 %) at top left, (ii) (80 %, 20 %) at top right, (iii) (70 %, 30 %) at bottom left, (iv) (50 %, 50 %) at bottom right, respectively

where k is wave number, ω is angular frequency, ϕ_i is phase and E_i is amplitude of electric field, which is linear to square root of beam intensity I_i . In these formulas, the sign of the second term is minus in the cases of *c* and *d* beams.

The parameters are intensity and phase, as summarized in Table 1. The beam intensity E_{i0} was set to 1 or 0.5, and phase shift ϕ_i was 0, $\frac{1}{4}\pi$, $\frac{2}{4}\pi$, $\frac{3}{4}\pi$ or π . It should be noticed that there are huge numbers of axial-symmetric, point-symmetric patterns, which are summarized in six figures composed of 21 interference patterns. The shapes of higher- and lower-fluence regions are also summarized in the table. In this simulation, wavelength is set to 785 nm, and θ is set to 14.6° according to past experiment [5, 6].

3 Results and discussion

The interference pattern variation as a function of phase shift of three beams, corresponding to the phase shift of one beam, is shown in Fig. 1. The top pictures are simulated interference patterns, where the red region represents higher fluence, and the violet region represents lower fluence. The

sets of four pictures in the middle are contour plots of corresponding interference patterns at different thresholds, which is explained in the bottom inserts. In the case of top left picture in a box of right insert, the beige region is irradiated at higher fluence over 90 % of peak fluence. On the other hand, violet region is irradiated at lower fluence under 10 %. These thresholds vary for the pictures; (i) (90 %, 10 %) at top left, (ii) (80 %, 20 %) at top right, (iii) (70 %, 30 %) at bottom left, (iv) (50 %, 50 %) at bottom right, respectively. The contour lines for different thresholds appear at different conditions such as fluence of interfering laser, film thickness etc. These shapes of the areas have strong correspondence or relation to the resultant matrix pattern.

In the case without phase and amplitude modulation between the beams, a uniform interference pattern in lattice are formed, as shown in Fig. 2(a). The higher-fluence region has circle or round box shape. In practical processing, this area corresponds to a nanohole or a 3-dimensional structure such as nanobump, nanowhisker, nanowaterdrop etc. [3, 5, 7, 8]. The residual area, which corresponds to nanomesh, is negative of higher-fluence area. When phase shift is added to a beam or three beams equally, residual peak appears between the original peaks, as shown in Fig. 2(b), (c) and (d). In the

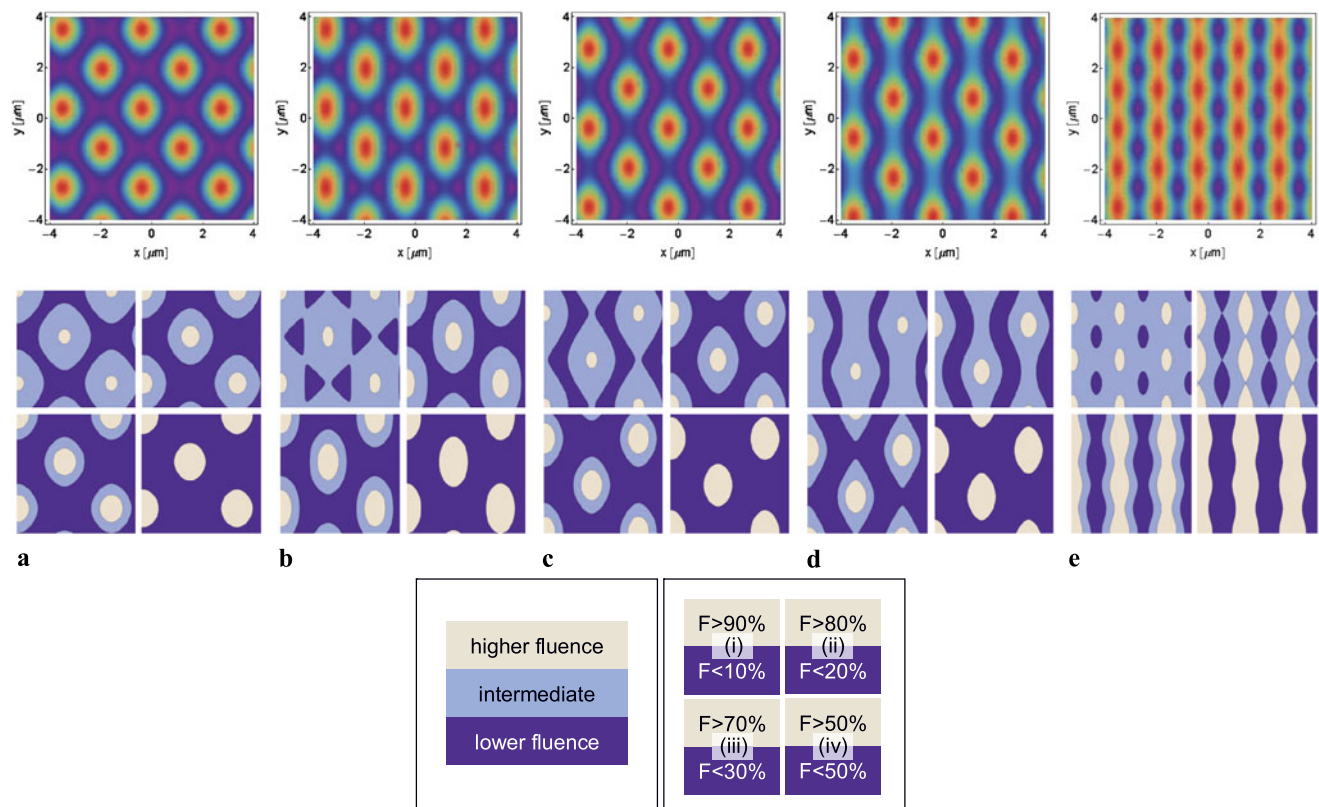


Fig. 3 (a), (b), (c), and (d) Ellipsoidal mesh, triangle mesh in hexagon, wave. (e) Ellipse, cat's eye and pea

case of $\frac{2}{4}\pi$ phase shift as shown in Fig. 2(c), the lower-fluence region seems to four countering ellipses, which is shown in the counter plot (i). In the case of $\frac{3}{4}\pi$ phase shift as shown in Fig. 2(d), the lower-fluence region seem to four countering boxes, which is shown in the counter plot (iii). At π phase shift, as shown in Fig. 2(e), the density of peak is doubled compared to the case without phase shift shown in Fig. 2(a). The method for forming a dense pattern in a single shot is very important in practical point of view. At counter plot with threshold 50 % shown in (iv), the higher- and lower-fluence regions show check patterns.

In Fig. 3, ellipsoidal patterns and connected peaks are categorized. In Fig. 3(a), slightly ellipsoidal pattern can be obtained, though the intensities of the beams are equal. Here, ellipsoidal patterns have been obtained by modulate amplitude between the beams [3]. In Fig. 3(b), both amplitude and phase are modulated. The higher-fluence region has ellipsoidal shape. It is interesting that six triangle meshes in hexagonal matrix are surrounding a peak, as shown in the contour plot (i). It is peculiar compared to the normal interference pattern, where four meshes in tetragonal matrix are surrounding a peak, as shown in Fig. 1. This technique is important because the array pattern strongly affects the character of the metamaterial. In case of Fig. 3(c), the shape of ellipsoid is a bit sharper compared to Fig. 3(b). The lower-fluence region forms a wave structure, as shown in (i). The

process window of the formation of wave structure is wider in the case of Fig. 3(d), where such structures can be seen in both (i) and (ii). In case of Fig. 3(e), higher- and lower-fluence regions have the same patterns. The shapes are like a cat's eye in (ii). They are like peas in (iii) and (iv), which are connected peaks and holes.

Droplet structures of higher-fluence region, in which the direction of gravity is changed, are formed as shown Fig. 4(a), (b), (c), and (d). In the case of diagonal gravity, the peaks connect each other, as shown in Fig. 4(e). This pattern is slightly different from the base pattern shown Fig. 2(a), but the parameters are quite complicated.

A quite interesting pattern, which we named “peanuts”, is shown in Fig. 5. Two adjoining peaks of double density structure are jointed, and the characteristic patterns are formed. The lower-fluence region shows six round triangles in hexagonal matrix, as shown in the contour plot (iii). The direction of peanuts can be rotated by 90° as shown in Fig. 5(b). Moreover, the negative pattern of Fig. 5(b) can be obtained, as shown in Fig. 5(c).

In Fig. 6, peaks of double density pattern are joined in a different way compared to Fig. 5. The structure is like a “step” as shown in (iii) and (iv). The shapes of higher- and lower-fluence regions are like half-moon, which is shown in (ii).

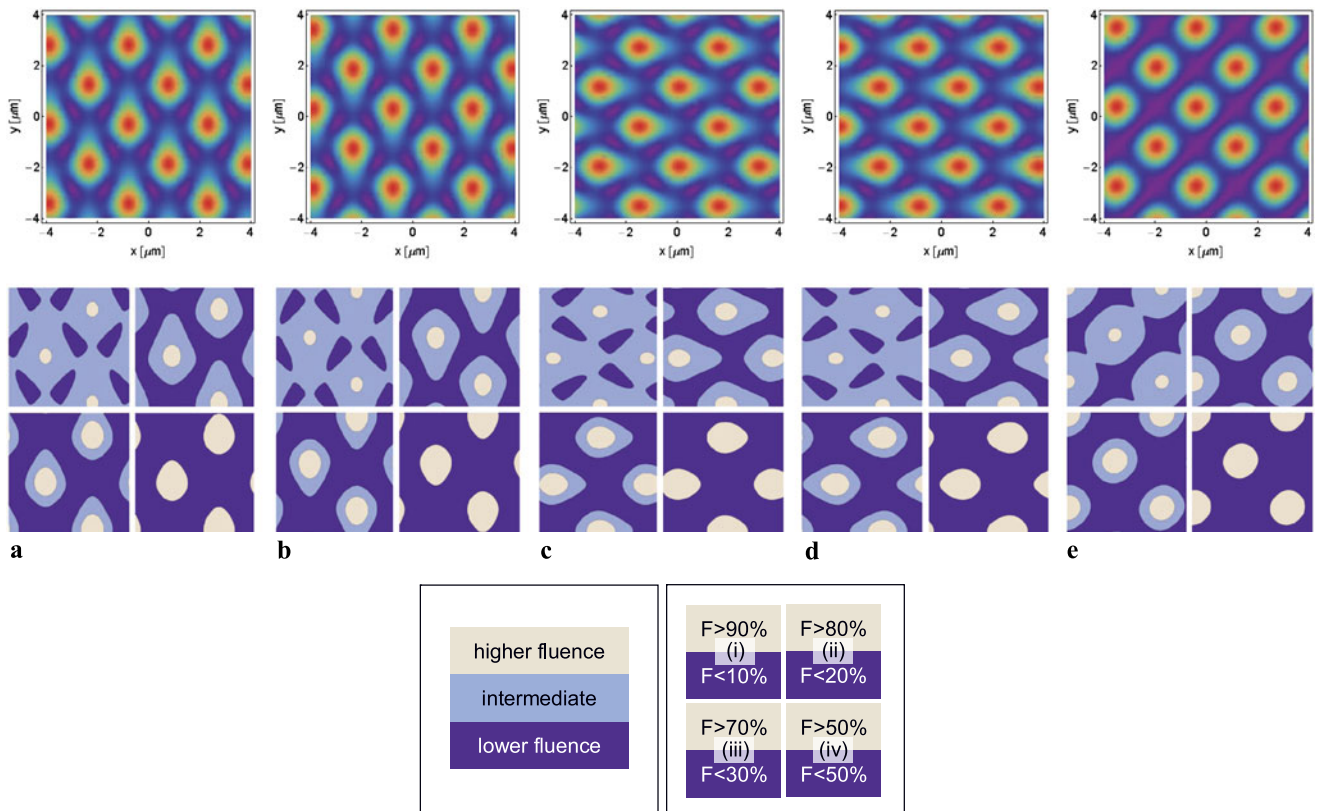


Fig. 4 (a), (b), (c), and (d) Droplet structures with different directions. (e) Pea, ellipse, star cross

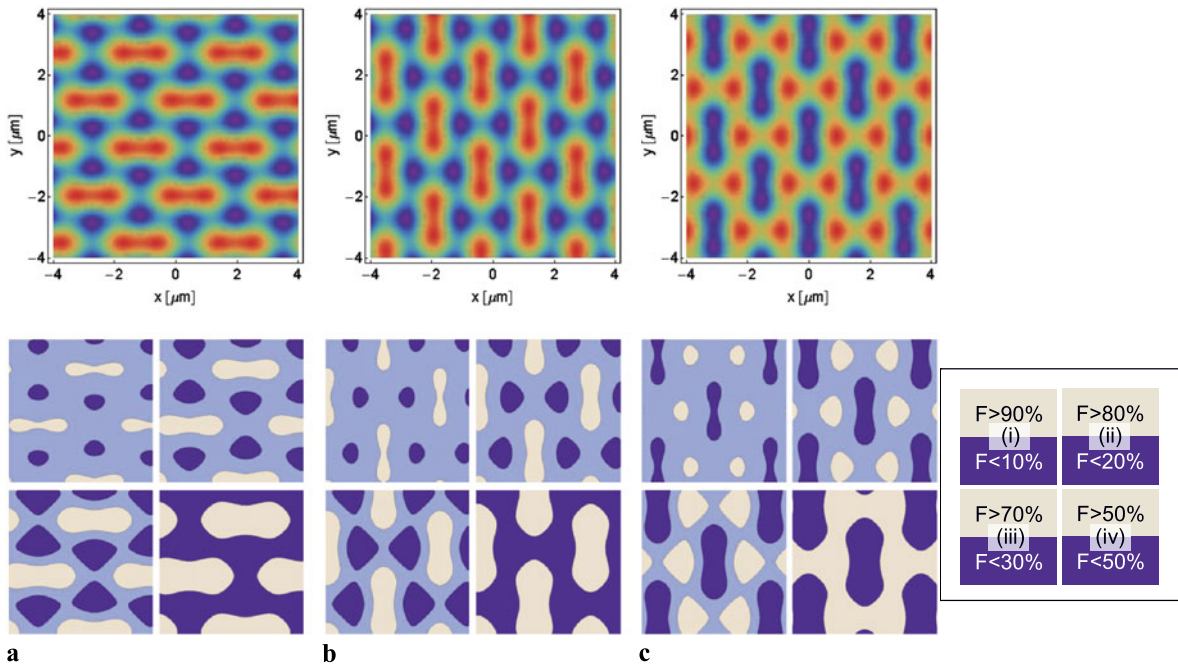


Fig. 5 Peanuts structures. (a) Horizontal, (b) vertical and (c) negative of (b)

In Fig. 7, unit structures are asymmetric in rotation, as in the case of Fig. 4. In the case of Fig. 7(a), the lower-fluence region seems to be a boomerang, as shown in the contour

plots (iii) and (iv). On the other hand, it is like connected gulls in the case of Fig. 7(b), which is clear in the contour plots (iii) and (iv).

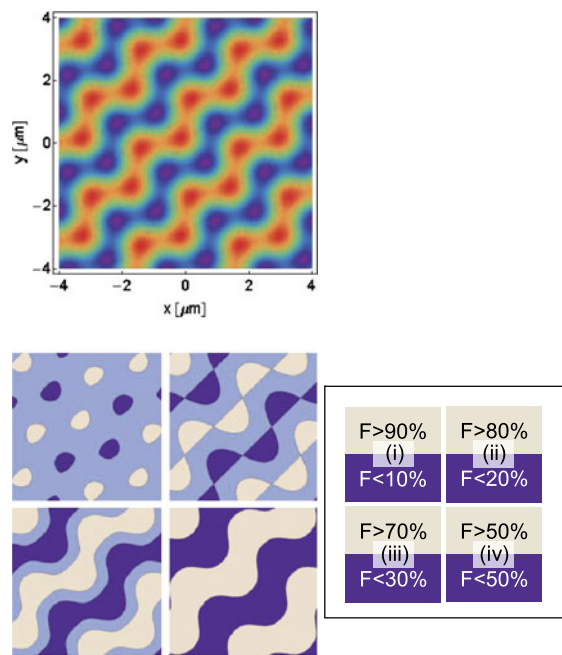


Fig. 6 Round half-moon, wave, step

From a practical point of view, the size and period between the unit structures is closely related to the corresponding wavelength of the metamaterial. For example, the smallest diameter of MHA we have made in the past experiment is 680 nm [9], and the corresponding wavelength would be at near-infrared. In general, period and unit size can be controlled by changing the interfering angle and fluence in our technique. In addition, a second- or third-harmonic wave of femtosecond laser will be useful for demagnification. In total, the practical wavelength can range from visible to terahertz.

In summary, a variety of interference patterns can be obtained by the combinations of only four beams. The unit figures of higher- or lower-fluence region are circle, ellipsoid, box, triangle, wave, cat's eye, pea, droplet, half-moon, boomerang, gull, and peanuts. They are in a tetragonal or hexagonal matrix, or axial-symmetric. In practical processing, there is one more degree of freedom: concave and convex structures. The number of combinations is huge, considering the target structure. By combining the patterns in the case of six beams [13], the flexibility of design of nanostructures in matrix will open a new aspect of metamaterial science.

Acknowledgements This research was financially supported by the Japan Society for the Promotion of Science (JSPS) Grant-in-Aid for Scientific Research (B) (no. 23360035) and Grant-in-Aid for Scientific Research on Innovative Areas (no. 23109509); the Amada Foundation for Metal Work Technology; and the Murata Science Foundation.

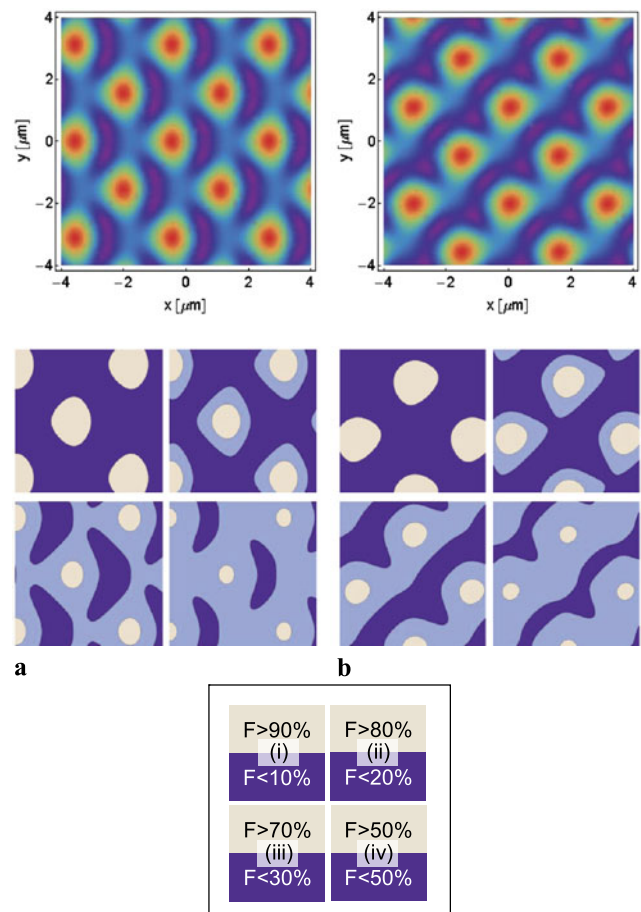


Fig. 7 (a) Boomerang, (b) Gull

References

1. Y. Nakata, T. Okada, M. Maeda, *Appl. Phys. Lett.* **81**, 4239 (2002)
2. Y. Nakata, T. Okada, M. Maeda, *Appl. Phys. A* **79**, 1481 (2004)
3. Y. Nakata, T. Okada, M. Maeda, *Jpn. J. Appl. Phys.* **42**, L1452 (2003)
4. Y. Nakata, N. Miyanaga, T. Okada, *Appl. Surf. Sci.* **253**, 6555 (2007)
5. Y. Nakata, T. Hiromoto, N. Miyanaga, *SPIE Newsroom* (2009). doi:10.1117/2.1200906.1708
6. Y. Nakata, K. Tsuchida, N. Miyanaga, H. Furusho, *Appl. Surf. Sci.* **255**, 9761 (2009)
7. Y. Nakata, T. Hiromoto, N. Miyanaga, *Appl. Phys. A* **101**, 471 (2010)
8. Y. Nakata, K. Momoo, T. Hiromoto, N. Miyanaga, *Proc. SPIE* **7920**, 79200B (2011)
9. Y. Nakata, N. Miyanaga, T. Okada, *J. Phys. Conf. Ser.* **253**, 245 (2007)
10. H.M. Phillips, D.L. Callahan, R. Sauerbrey, G. Szabó, Z. Bor, *Appl. Phys. Lett.* **58**, 2761 (1991)
11. A.A. Maznev, T.F. Crimmins, K.A. Nelson, *Opt. Lett.* **23**, 1378 (1998)
12. T. Kondo, S. Juodkazis, V. Mizeikis, S. Matsuo, H. Misawa, *New J. Phys.* **8**, 1 (2006)
13. Y. Nakata, K. Murakawa, K. Sonoda, K. Momoo, N. Miyanaga, *Appl. Opt.* **51**, 5004 (2012)